**Synthesis, structure and adsorption study on a Cu-succinic metal organic framework**

R. Roque-Malherbe [a,*], C. Rivera[a], R. Polanco[a], A. Rios and C. Lozano

School of Science, Universidad del Turabo, PO Box 3030, Gurabo, PR, 00778-3030, USA, arios@suagm.edu and clozano@suagm.edu

ABSTRACT

Our main purpose was the synthesis of a relatively thermally stable Cu-succinic metal organic framework (Cu-Su-MOF), their structural characterization and the investigation of their adsorption properties. The key questions of study were the determination of the Cu-Su-MOF thermal stability, their structure and the relation between framework expansion during high pressure adsorption and the structure of the degassed material. Thereafter, the as-synthesized and degassed materials were studied with scanning electron microscopy, energy dispersive X-ray analysis, diffuse reflectance infrared and Raman spectrometry, thermo-gravimetric analysis, X-ray diffraction, magnetic measurements and low and high pressure carbon dioxide adsorption. The main inferences made were the structure of the Cu-Su-MOF was shaped by a bis-monodentate bridging cooper 3 D framework exhibiting a monoclinic *Pm* lattice; this material has pores with diameters ca. 6 Å surrounded basically by oxide anions; the $Cu^{2+}$ ions linked to the succinate anion in octahedral coordination, saturated with the oxygen belonging to the *COO-* anion; the micropore volume measured at low pressure was *W = 0.131 cm3/g* while at high pressure this parameter was, *W = 0.255 cm3/g*; where the framework expansion was due to the cooperative interaction of the carbon dioxide adsorbed molecules with the framework and between them. Since the tested material possess a strong to moderate interaction with the adsorbed gas, fast gas transport, high adsorption capacity, and high thermal and mechanical stability can be concluded that the synthesized Cu-MOF could be a thermally stable, selective to small molecules, with moderate adsorption interaction, small regeneration temperature and moderately high pore volume adsorbent.

a. Present address: Materials for Science and Art Use, PO Box 2017, PMB 405, Las Piedras, PR 00771, USA. rroquemalh@aol.com, christymarierivera@gmail.com and polancoramon@gmail.com

*. R. Roque-Malherbe, corresponding author.

## 1. INTRODUCTION

Metal-organic frameworks (MOFs) are materials consisting of metal nodes and organic spacers, showing permanent porosity [1-3]. The methodology for the synthesis of these zeolite-like compounds was created in the first years of the 1990's [4,5]. After that, an exponential growth of new MOFs has been steadily produced, to be used, in catalysis [6], gas adsorption [7], separations [8] and further applications [9]. However, the chemical and thermal stability of these materials is less than other adsorbents, such as: zeolites, silica, alumina and activated carbons; therefore, is necessary to find procedures to produce more stable MOFs. In this regard, the succinate anion can be very attractive as a spacer [10,11], to produce MOFs [12,13] with relatively high thermal stability.

In particular, adsorption is a very useful property for the practical application of MOFs [2,14] and other porous polymeric materials [15]. Additionally, it could be also a characterization tool to investigate the surface chemistry together with the adsorption space geometry of porous materials [19-22]. In this regard, been carbon dioxide an excellent test molecule; given that, it is generally strongly adsorbed within the dispersion, $\phi_D$, repulsion, $\phi_R$, and field gradient quadrupole, $\phi_{EQ} = (\partial E/\partial z)(Q_{CO_2}/2)$ (where, $(\partial E/\partial z)$ is the electric field gradient and $Q_{CO_2}$ the quadrupolar moment) potential fields; hence, owing to the relatively high quadrupolar moment ($Q_{CO_2}$ = - 4.3 × $10^{-42}$ C.$m^2$) presented by this molecule the interaction with surfaces is normally significant [18].

Furthermore, the adsorption process can produce the deformation of the adsorbent [23]; i.e., the solid adsorbent is not inert during the course of the adsorption processes, thus, it can experience, expansion, contraction and swelling [24-27]. In this regard, a group of porous materials known as soft porous crystals (SPC) have been investigated on account of their structural flexibility, giving that, these materials undergo different framework

transformations produced by external stimuli, such as, mechanical stress, adsorption or temperature [14,16,24,25]. Moreover, in some cases, the interaction of the guest molecules with the framework produce atypical adsorption-desorption isotherm patterns; for instance, the so called gate opening effect characterized by a big hysteresis loop between the adsorption and desorption branch of the isotherm [26,27].

In conclusion, the main purposes of the research reported in the present paper were: synthesis, elucidation of the structure, study of the framework expansion during carbon dioxide adsorption and thermal stability of the produced Cu-succinic metal organic framework, hereby labeled Cu-Su-MOF. To meet the objectives related to the elucidation and thermal stability of the structure, the synthesized material was investigated with, scanning electron microscopy (SEM), powder X-ray diffraction (PXRD), energy dispersive X-ray analysis (EDAX), diffuse reflectance infrared and Raman spectrometry (DRIFTS and RS), thermo-gravimetric analysis (TGA), and physical adsorption at low pressure (up to 0.1 MPa). Thereafter, to further understand the framework expansion effect during high pressure adsorption, was applied an approach based in the osmotic theory of adsorption [14, 17].

## 2. EXPERIMENTAL SECTION

### 2.1. Materials and Synthetic Procedure

The chemicals used in the synthesis were all of analytical grade without additional purification; whereas, water was bi-distilled. The synthesis procedure was: 1 mmol of $Cu(NO_3)_2$ and 1 mmol of succinic acid ($C_4H_6O_4$) were dissolved in 50 ml of dimethylacetamide (DMA, $CH_3CON(CH_3)_2$)); afterwards, to the previous solution were added 29 ml of $H_2O_2$ (50 %); next, the mixture was cooled adding 24.1 ml of a 70.3 mM

triethylamine (TEA, $N(CH_2CH_3)_3$) solution in DMA. Later, the flask was sealed and placed in a hood for 24 h. at a temperature of 70 $^0$C. Finally, the product was washed with distilled water and dried at 70 $^0$C.

### 2.2 Methods

First of all, the scanning electron microscopy (SEM) study was carried out with a JEOL JSM-6360, microscope whose electron beam acceleration voltage was 20 kV. The tested sample grains were homogeneously placed on a carbon tape; hence, images of the tested materials were acquired. In addition, the elemental chemical analysis of the as-synthesized and washed samples, were performed using an EDAX spectrometer coupled into the microscope.

Secondly, the XRD profiles were gathered with a Bruker D8 Advance system in Bragg-Brentano vertical goniometer configuration. The 2θ angular measurements were made by applying steps of 0.01 degree. The X-ray radiation source was a ceramic Cu anode tube. Variable Soller slits were included and a Ni filter was placed, prior to the detector. Additionally, a LynxEye™ one-dimensional detector was used to produce large counting that resulted to high quality XRD profiles which can be accurately resolved by least square methods [16]. To confirm the proposed structure, the gathered XRD patterns were refined with the Pawley and Rietveld methods; in this regard. the computer program used to perform the refining processes was the Bruker DIFFRAC*plus* TOPAS™ software package; where, the emission profile was shaped by Lorentzians [14].

Afterwards, diffuse reflectance infrared Fourier transform spectra were gathered using a Thermo Scientific Nicolet iS10 FTIR spectrometer. The data were collected at a resolution of 4 $cm^{-1}$ employing 100 scans per sample. The hydrated samples spectra were obtained at room temperature under $N_2$ flow (Praxair, 99.99 %) at a rate of 50 cc/min. To get the spectra of the dehydrated samples, they were heated, up to 100 $^0$C, under a flow of $N_2$ (Praxair, 99.99 %) at

a rate of 50 cc/min for 2 hours [20]. The spectra of the dehydrated materials were then obtained at room temperature, under $N_2$ (Praxair, 99.99 %) flow at a rate of 50 cc/min. In addition, DRIFTS spectra of carbon dioxide adsorbed in the MOF framework were obtained using as background the dehydrated sample at room temperature [21]. After that, $CO_2$ (Praxair, 99.99 %) flow at a rate of 50 cc/min for three minutes was passed through the dehydrated samples; then, the sample was purged under $N_2$ (Praxair, 99.99 %) flow at a rate of 50 cc/min for one minute [22]. The spectrum of the carbon dioxide molecule adsorbed on the PBA microporous framework, were then obtained at room temperature under $N_2$ flow.

The micro-Raman spectra were collected with a Jobin-Yvon T64000 Raman spectrophotometer, consisting of a double pre-monochromator coupled to a monochromator/spectrograph with 1800 grooves/mm grating. A Leica microscope with an 80X objective, was applied to focus the 514.5 nm radiation of an $Ar^+$ laser.

Meanwhile, the magnetization curves (M versus H) were collected at room temperature (298 K) in the vibrating sample magnetometer (VSM), Lakeshore 7400 Series [20]. The powder sample was weighted, located on the sample holder and subsequently used the ramp from -2.2 to 2.2 T and backward directions.

Afterwards, the thermos-gravimetric analysis (TGA) was carried out with a TA, Q-500 instrument [22]. The temperature of the sample was scanned, from 25 to 700 C, at a constant heating rate (5 C /min), using a flow of 100 ml/min of pure $N_2$. The TGA data was collected as Weight per-cent (*Wt. %*) versus T (0C), where, $W_t = (M_t/M_0)100$, $M_t$., is the sample mass at temperature, T and the initial mass of the sample is $M_0$ .

Lastly, carbon dioxide (Praxair, 99.99 %) adsorption was investigated at 273 K and 300 K in the low pressure (LP) range (pressure up to 1 bar) on samples degassed at 373 K for four hours in high vacuum ($10^{-6}$ Torr) in a Quantachrome AS-1 automatic sorption analyzer [16]. To measure the carbon dioxide (Praxair, 99.99 %) adsorption at temperatures of 273 K, 300

K and 318 K on samples degassed at 373 K for four hours in high vacuum ($10^{-6}$ Torr) in the high pressure range (pressure up to 30 bar) a Quantachrome iSorbHP-100 was used. The backfilling process was performed using helium (Praxair, 99.99 %) in both cases.

Finally, the curve fitting processes were performed with the analysis and peak separation software PeakFit® (Seasolve Software Inc., Framingham, Massachusetts) based on a least square procedure using the method developed by Levenberg and Marquardt, making possible the calculation of the best fitting parameters.

## 3. RESULTS AND DISCUSSION

### 3.1. Synthesis

The synthesis was made in dimethylacetamide (DMA, $CH_3CON(CH_3)_2$) as solvent, the organic spacer was succinic acid ($C_4H_6O_4$) and the source of the metal node was cooper nitrate ($CuNO_3$). Additionally, hydrogen peroxide ($H_2O_2$) was used as catalyst and thriethylamine (TEA, $N(CH_2CH_3)_3$) was added, to remove hydrogen from the dicarboxylic acid.

### 3.2. Characterization

**3.2.1. SEM study**. The micrograph of the as-synthesized Cu-MOF are reported in Fig.1;. these images exhibited the formation of a highly crystalline material presenting coffin shaped crystals, 1-6 μm wide and long and, 1-1.5 μm high. Along with the SEM study a qualitative EDAX elemental chemical analysis of the as-synthesized Cu-Su-MOF was performed. This analysis revealed the presence of, carbon, oxygen, nitrogen and cooper in the tested sample.

**3.2.2. Crystallographic analysis**: the powder X-ray diffraction patterns of the degassed materials were collected "in situ" in a high temperature chamber under $N_2$ flow at 298 K (as-synthesized), and degassed at 373 K, 448 K, 473 K, 523 K and 573 K (Fig. 2). These profiles were fitted with the Pawley method using the Bruker DIFFRAC*plus* TOPAS™ software; so the refining process made possible the calculation of the cell parameters for the tested material degassed, at different temperatures. After all, the best fitting parameters calculated, were obtained when the monoclinic *Pm* space group was assumed in the refining process (Table 1). Additionally, as a final point, is necessary to state that was observed a structural collapse of the degassed material at 573 K (Fig. 2).

**3.2.3. Evaluation of the tested material with infrared spectroscopy:** alike the XRD research the DRIFTS study was made at different temperatures, in degassed samples; that is, the spectra of the as-synthesized Cu-Su-MOF (room temperature, 298 K) and degassed at different temperatures (373, 448 and 523 K) were collected "in situ" in a high temperature IR cell under $N_2$ flow. In this regard, the corresponding spectra are shown in Figs. 3 a and b, in which on the one hand the characteristic absorption bands of the -COO- groups [28], located on 1450 and 1650 $cm^{-1}$ are observed in the spectrum shown in Fig. 3 a; while a broad band (3200-3700 $cm^{-1}$) was observed in the spectrum reported in Fig. 3 b; similarly, at higher temperatures, i.e., 447 and 523 K, the broad band disappeared; thereafter, since this band corresponded to the stretching vibrations produced by adsorbed $H_2O$ and included TEA molecules; therefore, these components disappeared after degassing at 447 and 523 K; whereas since the bands in the range 2700-3300 $cm^{-1}$, produced by the vibrations corresponding to DMA [29] also vanished after degassing at the previously reported temperatures, hence this compound was also released.

**3.2.4. Raman investigation:** the room temperature Raman spectrum of the as-synthesized Cu-Su-MOF is reported in Fig. 4b, showing a band located on ca. 490 $cm^{-1}$ which is

particularly distinctive of the stretching vibration mode of $CuO_6$ octahedra, corresponding to $Cu^{2+}$ ions linked to the succinate in bidentate mode [34], i.e., was synthesized a Cu-succinic material..

**3.2.5. DRIFTS carbon dioxide adsorption investigation:** the collected infrared spectrum of carbon dioxide adsorbed at 760 Torr and 298 K on the tested Cu-Su-MOF is reported in Fig. 4a; in this spectrum the corresponding absorption band observed at ca. 2339 $cm^{-1}$ is the result of the attachment of the carbon dioxide molecule by dispersive and electrostatic forces to the adsorption space defined by the Cu-Su-MOF pores, where the adsorption process produces the confinement of the carbon dioxide molecule, hence the frequency shifts from 2349 $cm^{-1}$ to 2339 $cm^{-1}$; similarly, the band at ca. 2321 $cm^{-1}$ is assigned to a combination band [30]; these assignments are consistent with the symmetry shown by the free carbon dioxide molecule, i.e., the $D\infty h$ group symmetry; which exhibits four fundamental vibration modes; that is, the symmetric stretching, $\nu_1$ at 1338 $cm^{-1}$, the doubly degenerate bending vibration, $\nu_{2a}$ and $\nu_{2b}$ (667 $cm^{-1}$), and the asymmetric stretching vibration $\nu_3$ located at 2349 $cm^{-1}$ [30-32]; where, the, $\nu_2$ and $\nu_3$, modes are infrared active, whereas the $\nu_1$ is only Raman active in the free molecule, while the asymmetric stretching vibration, $\nu_3$, corresponds to carbon dioxide physically adsorbed [31]. Additionally, since carbon dioxide is amphoteric, it interacts with acid and basic surface sites, hence another band must be normally observed at ca. 2362 $cm^{-1}$ [32]; in the present case, this band should correspond to adsorption of carbon dioxide on an electron accepting Lewis acid site forming the following adducts, $Cu^{2+}$ ••• $O = C = O$ [33]; giving that, this band was not observe, hence, their absence indicated that the $Cu^{2+}$ ions are saturated by the oxalate oxygen atoms.

**3.2.6. Magnetic properties of the synthesized material**: the magnetization curves of the as-synthesized Cu-Su-MO, together with those of a well characterized Ni-nitroprusside (labelled

Ni-NP) sample [20] used as a standard for the calibration of the vibrating sample magnetometer are reported in Fig. 5; in this regard, the effective magnetic moment reported in literature for the Ni-NP is, $\mu_{eff}$ = 2.9 $\mu B$, ($\mu B$, Bohr magnetron) [20, 35], subsequently, the effective magnetic moment for the Cu-Su-MOF yielded, $\mu_{eff}$ = 2.15 $\mu B$, when compared with the Ni-NP sample used as a standard (Fig. 5); accordingly, given that $Cu^{2+}$ in octahedral coordination exhibits magnetic moments in the following range, 1.7 < $\mu_{eff}$ < 2.2 [36], hence, we conclude that the metallic node in the MOF framework is $Cu^{2+}$ in octahedral coordination as was also demonstrated by the Raman study.

**3.2.7.**: **Geometry of the adsorption space of the tested MOF:** to measure the microporore volume was applied an adsorption isotherm equation, formally identical to the Langmuir isotherm [17, 18] but describing volume filling rather than surface recovery [37]; i.e. [38]:

$$n_a = \frac{N_a KP}{1+KP} \qquad (1)$$

Where, $K_I = K_0 \exp\left([(E_0^g - E_0^a)]/RT\right)$ is a constant for $T = const$, $E_0^g$ is the reference energy state for the gas molecule, $E_0^a$, is the reference energy state for the adsorbed molecule in the homogeneous adsorption field inside the cavity or channel, $n_a$, is the amount adsorbed and, $N_a$, is the maximum amount adsorbed in the volume of the micropore. In linear form this equation is expressed as follows:

$$y = P = N_a\left(\frac{P}{n_a}\right) - \frac{1}{K(T)} = mx = b \qquad (2)$$

On this ground, the experimental carbon dioxide adsorption data at 298 K on Cu-Su-MOF samples degassed at 373 K, 448 K and 473 K were linearly fitted by equation “2”, yielding the linear plots reported in Fig. 6a. The fitting of these plots made possible the determination of the maximum amount adsorbed (Table 2); therefore, the micropore volume was calculated

using the Gurtvich rule, i.e., $W_{MP}^{CO_2} = V_{CO_2}^{L} N_a$; where, $V_{CO_2}^{L} = 48.3\, cm^3 / mol$, is the molar volume of carbon dioxide.

As another means for the study of the geometry of the adsorption space, was collected the thermal gravimetric (TG) profile of the Cu-Su-MOF; this profile, reported in Fig. 6 b, evidenced features related to the consecutive liberation of adsorbed water, up to ca. 393 K, in two steps, later, DMA was released, up to ca. 465 K, also in two steps, then, was observed the release of TEA together with the succinate decomposition. The combination of the low pressure adsorption and TGA data made possible to conclude that was synthesized a metal organic framework, since the produced material was porous, besides the amount of water released up to 400 K indicated that the mcropore volume of the Cu-SU-MOF is 0.21 $cm^3$/g, a value similar to those measured using carbon dioxide adsorption (Table 2)

### 3.3. Structure elucidation

The succinate anion as other dicarboxylic acids have many potential donor sites to produce different coordination modes including bidentate-chelate, monodentate-chelate, monodentate-bidentate, bis-monodentate and bis-bidentate bridgings [11]. Hence, using the data provided by the XRD, TGA, DRIFTS, Raman and adsorption results, the knowledge related to the linking options of succinic acid as spacer [12, 13] and $Cu^{2+}$ as node [9], the unit cell parameter reported for the material degassed at 448 K (Table 1) and the atomic positions, Wyckoff sites and occupancy factors, registered in the International Tables for Crystallography [39] (Table 3), was proposed a monoclinic *Pm* space group unit cell representation for the structure of the dehydrated Cu-Su-MOF framework with chemical formula $CuC_{12}O_{12}H_{18}$ (Fig. 7, H was not included).

Next, for the confirmation of the proposed structure, in Fig. 8a, is presented the XRD profile of the dehydrated Cu-Su-MOF, simulated with the PowderCell software [40], assuming the

monoclinic *Pm* space group unit cell representation, the atomic positions, Wyckoff sites and occupancy factors reported in Table 3 [39], along with the unit cell parameter reported for the material degassed at 448 K (Table 1) exhibiting the following chemical formula $CuC_{12}O_{12}H_{18}$ (H was not included). It is palpable that the simulated profile closely resembles the experimental one (Fig. 1).

Finally, the XRD diffraction pattern of the Cu-Su-MOF was fitted with the Rietveld method using the Bruker AXS TOPAS® software package and the data reported in Table 3. The fitting process was performed while the atomic position, occupancy factors and isotropic thermal factors for the cations and anisotropic thermal factors for the oxygen ions were kept fixed and the cell parameters refined. The calculated cell parameters reported in Table 4 were, within the experimental error the same reported in Table 1.

To conclude is possible to affirm that the simulation together with the Rietveld fitting of the XRD profile validated the framework structure, proposed for the Cu-Su-MOF.

### 3.4. High pressure adsorption study

In Fig. 9a the data corresponding to the high pressure carbon dioxide adsorption (Ad.) and desorption (Des.) isotherms, at 273 K and 298 K on the Cu-Su-MOF, degassed at 448 K are shown. In this regard, to calculate some parameters characterizing carbon dioxide adsorption on the Cu-SU-MOF, the data reported in Fig 9a was fitted to the Dubinin- Radushkevitch (D-R) adsorption isotherm equation; hence, to carry out the process was used the linear form of the D-R isotherm equation [37]:

$$\ln(n_a) = \ln(N_a) - \left(\frac{RT}{E}\right)^2 \left[\ln\left(\frac{P_0}{P}\right)\right]^2 \qquad (3)$$

In which $n_a$ is the amount adsorbed, $P/P_0$ is the relative pressure, where $P$ is the adsorption equilibrium pressure, $P_0$ is the vapor pressure of carbon dioxide at 298 K, $E$ is a parameter

known as the characteristic energy of adsorption, and $N_a$ is the maximum amount adsorbed in the micropore volume. The linear fitting of the high pressure adsorption data of carbon dioxide at 273 K and 298 K on the Cu-Su-MOF dehydrated at 448 K (Fig 9b) by equation (3) made possible the determination of the characteristic energy of adsorption and the maximum adsorption magnitude $N_a$; where, the micropore volume was calculated using the Gurtvich rule (Table 5). These data allowed us to acknowledge the sorbent deformation effect [24], giving that the micropore volume calculated with the high pressure data is bigger than the micropore volume determined with low pressure isotherms (Tables 2 and 5).

Now, an assumption is made, specifically, the adsorbent plus the adsorbed phase is considered a solid solution, the adsorbate-adsorbent system (*aA*); thereafter, the fundamental thermodynamic equation, within the frame of the solution thermodynamic approach, is given by [41,42]:

$$dU_{aA} = TdS_{aA} - PdV_{aA} + \mu_a dn^a + \mu_A dm \qquad (2)$$

Where, $U_{aA}$ , $S_{aA}$ and $V_{aA}$ are the internal energy, entropy and volume of the system *aA*, while $\mu_a$ (in *J/mol*) and $\mu_A$ (in *J/Kg*) are the chemical potentials of the adsorbed and solid phases in the solution and, $n^a$ , and *m* the amount of moles of adsorbate and the adsorbent mass in the system *aA*. Hence [41]:

$$U_{aA} = TS_{aA} - PV_{aA} + \mu_a n^a + \mu_A m \qquad (3)$$

On this ground, is possible to write the internal energy per unit mass of adsorbent as follows: $\overline{U}_{aA} = T\overline{S}_{aA} - P\overline{V}_{aA} + \mu_a n_a + \mu_A$; where, $n_a = n^a / m$. Now the internal energy for the unit mass of empty adsorbent is given by: $\overline{U}_A = T\overline{S}_A - P\overline{V}_A + \mu_A^0$ . Therefore [41,42]:

$$U_a = \overline{U}_{aA} - \overline{U}_A = TS_a - PV_a + \mu_a n_a + \Phi \qquad (4)$$

Where, $S_a = \overline{S}_{aA} - \overline{S}_A$ , $V_a = \overline{V}_{aA} - \overline{V}_A$ and $\Phi = \mu_A - \mu_A^0$. Likewise, the fundamental thermodynamic equation for the adsorbed phase is given by:

$$dU_a = TdS_a - PdV_a + \mu_a dn_a + d\Phi \qquad (5)$$

Therefore, since the Grand potential is defined as: $\Omega = U - TS - \mu n$, hence: $\Omega_a = U_a - TS_a - \mu_a n_a - \Phi$; then

$$d\Omega_a = dU_a - TdS_a - S_a dT - d\mu_a n_a - \mu_a dn - d\Phi \qquad (6)$$

Consequently, substituting equation "5" in equation "6" we get: $d\Omega_a = -PdV_a - S_a dT - n_a d\mu_a$ . Now, in equilibrium: $d\mu_a = d\mu_g = RT \ln f$ , where *f*, is the fugacity of the adsorbate, thereafter:

$$d\Omega_a = -PdV_a - S_a dT - n_a RT \ln f = d\Phi \qquad (7)$$

But since, $\Omega_a = \Phi$, then, for *T* = *const*:

$$\Phi = RT \int_0^f n_a d(\ln f) - V_a P \qquad (8)$$

In the frame of the osmotic theory of adsorption [41], $\Phi = \Pi W$, hence:

$$\Pi W = RT \int_0^f n_a d(\ln f) - V_a P \qquad (9)$$

Where, *W*, is the micropore volume of the adsorbent and, $\Pi = P_0 - P$, is the osmotic pressure where $P_0$, is a pressure that can compress the adsorbate and produce the same effect created by an adsorption field, i.e., an amount, *na*, of molecules [18]. However, since the experimental pressure was not very high hence we used the following approximate relation:

$$\Pi W = RT\int_0^P n_a d(\ln P) \qquad (10)$$

Where, $W$, $n_a$ and $P$ are respectively, the micropore volume, the magnitude of adsorption and the equilibrium pressure, and $\Pi = P_0 - P$, is the osmotic pressure [17,42]. The physical meaning of, $\Pi$ can be explained by a model, where it is assumed that the adsorption field within the adsorption space is zero, explicitly we have a mere geometric volume, in this case a pressure $P_0$ can compress the adsorbate in this geometric volume and produce the same effect created by an adsorption field, i.e., an amount $n_a$ of molecules compressed in this volume [18]. Therefore, in Figs. 9c and 9d were plotted the pore volume ($W$) versus the osmotic pressure ($\Pi$) according to equation "10". These data show an initial state where the volume did not notably change, even though, at higher pressure it is evidenced a rapid increase of the micropore volume fact pointing to the deformation of the adsorbent during the adsorption process.

Since the carbon dioxide molecule has an ellipsoidal form, 5.4 Å long and with a diameter of 3.4 Å [43], hence, the adsorbate-adsorbent interactions are greatly dependent on the pore geometry, specially, in the case when the pore width of the adsorbent is very near to the size of the adsorbed molecules [44], thus, the cooperative interaction of the carbon dioxide molecules with the framework and between them, produces the osmotic pressure $\Pi$ that increases with the equilibrium adsorption pressure of $CO_2$ in the gaseous phase, causing the onset of sorbent deformation at $\Pi \approx 100$ MPa, at 273 K and $\Pi \approx 90$ MPa at 298 K. Then, an abrupt increase was possible owing to the well known flexibility of the succinate[45] linkers that shapes the framework. Conversely, at a low pressure range $n_a = K(T)P$, where $K(T)$ is a constant for $T$ = const. Therefore, using equation (4) is easy to show that, $\Pi W = n_a RT$, hence the adsorbed phase behaves as an ideal gas within the adsorption space at low pressure.

Lastly, the isosteric heat of adsorption *qiso* was calculated using the data reported in Fig. 9a, with a relation similar to the Clausius-Clapeyron equation [46]:

$$q_{iso} \approx RT^2 \left[ \frac{d \ln P}{dT} \right]_{n_a} \approx RT_1T_2 \left[ \frac{\ln P_2 - \ln P_1}{T_2 - T_1} \right]_{n_a} \qquad (11)$$

Where, $P_1$ and $P_2$ are the equilibrium adsorbate pressure at, $n_a$ = constant, for the temperatures $T_1$ and $T_2$. The results of these calculations are plotted in Fig. 9e; where, $\theta = n_a / N_a$ . Thereafter, since carbon dioxide is a molecule showing a noticeable quadrupolar moment like $CO_2$ ($Q$ = -4.3 10-42 Cm2 [47]) when it is adsorbed becomes subjected to the field gradient quadrupole together to dispersion and repulsion, acid-basic interactions, if acid or basic sites are present and sorbate-sorbate interactions. In our case the whole interaction was provided by the quadrupolar and dispersion interactions due to the absence of the adduct *Cu2+ ••• O = C = O* with the consequent lack of the acid-basic interaction [20-23], thereafter, the amount measured for the isosteric heat of adsorption, i.e., $q_{iso}$ = 26.1 kJ/mol, was not very high. Additionally, the constant value is caused by a compensation of the heterogeneity of the adsorption field and the sorbate-sorbate interactions [17,18]. Finally, for $\theta > 0.5$, the measured isosteric heat of adsorption abruptly decreased due to the deformation of the framework.

## 4. Conclusions

A great interest has been raised during the last years regarding the carbon dioxide concentration in the atmosphere. In recent times, between other adsorbents, MOFs have obtained great consideration as carbon dioxide adsorbents, due to their particularly high pore volume and the possibility to shape their pore structures [10]. Even though, MOFs can be unstable. In this regard, the main purpose of the reported research was the synthesis of a

relatively thermally stable Cu-succinic metal organic framework (Cu-Su-MOF), their structural characterization and the investigation of their adsorption properties. The key questions to be answered were the elucidation of the Cu-Su-MOF structure, its thermal stability, and the relation between framework expansion during high pressure adsorption and the structure of the degassed material. Thereafter, the as-synthesized and degassed materials were studied with scanning electron microscopy, energy dispersive X-ray analysis, diffuse reflectance infrared and Raman spectrometry, thermo-gravimetric analysis, X-ray diffraction, magnetic measurements and low and high pressure carbon dioxide adsorption. The main inferences made as a result of the analysis of the obtained data were: the structure of the degassed Cu-Su-MOF was shaped by a bis-monodentate bridging cooper 3 D framework exhibiting a monoclinic *Pm* lattice; this degassed material has pores with diameters ca. 6 Å surrounded basically by oxide anions; the $Cu^{2+}$ ions linked to the succinate anion were in octahedral coordination, saturated with the oxygen belonging to the *COO-* anion; the maximum micropore volume measured at low pressure was $W = 0.131\ cm3/g$ and at high pressure $W = 0.255\ cm3/g$, this framework expansion effect was due to the cooperative interaction of the carbon dioxide adsorbed molecules with the framework and between them, where this interaction was manifested as the osmotic pressure $\Pi$ whose increase caused the sorbent deformation; the value measured for the isosteric heat of adsorption in the low coverage range $0 < \theta < 0.5$, yielded $q_{iso} = 26.2$ kJ/mol, a moderate value.

Finally, since the tested material possess a strong to moderate interaction with the adsorbed gas, fast gas transport, high adsorption capacity, and high thermal and mechanical stability [22], we can conclude that with the synthesized Cu-MOF could be produced a thermally stable, selective to small molecules, with moderate adsorption interaction, small regeneration temperature and moderately high pore volume adsorbent. Besides, the gate effects (framework expansiom) proven by the hysteretic carbon dioxide desorption isotherms,

confirm the cooperative interaction of the carbon dioxide adsorbed molecules with the framework.

## 5. Acknowledgments

The authors acknowledge the financial support provided by the US Department of Energy through the Massey Chair project at the Universidad del Turabo and recognize the support of the National Science Foundation under the project CHE-0959334. We as well recognize the help provided by Dr. Pedro Fierro for the collection of the Raman spectrum and magnetization data, Dr. Frances Lugo for the SEM study, and Dr. A Hernandez and J. Primera-Pedroso for the collection of the adsorption data.

## 6. References


[1] D.J. Tranchemontangne, J.L. Mendoza-Cortes, M. O'Keeffe, O. M. Yaghi, Chem. Soc. Rev. **2009,** 38, 1257-21283

[2] J-R. Li,; Sculley, H-C. Zhou, Chem. Rev. **2012**, 112, 869-932.

[3] O.K. Farha, J.T. Hupp, Acc. Chem. Res. **2012**, 43, 1166-1175.

[4] B.F. Abrahams, B. Hoskins, R. Robson, J. Am. Chem. Soc. **1991**, 113, 3606-3607.

[5] M. Fujita, Y.J. Kwon, S. Washizu, S. Ogura, J. Am. Chem. Soc. **1994**, 116, 1151-1152.

[6] A. Corma, H. Garcıa, F.X. Llabres i Xamena, Chem. Rev. **2010,** 110, 4606-4655

[7] P. Horcajada, R. Gref, T. Baati, P.K. Allan, G. Maurin, P. Couvreur, G. Ferey, R.E. Morris, C. Serre, Chem. Rev. **2012**, 112, 1232-1268.

[8] K. Sumida, D.L. Rogow, J.A. Mason, T.M. McDonald, E.D. Bloch, Z.R. Herm, T-H. Bae, J.R. Long, Chem. Rev. **2012**, 112, 724-781.

[9] T.P. Maji, S. Kitagawa, Pure App. Chem. **2007**, 79, 2155-2177.

[10] F.A. Cotton, G. Wilkinson, C.A. Murillo, Advanced Inorganic Chemistry ($6^{th}$ edition), Wiley Interscience, New York, **1999**.

[11] T. Duangthongyou, S. Jirakulpattana, C. Phakawatchai, M. Kurmoo, S.; Siripaisarnpipat, Polyhedron **2010**, 29, 1156-1162.

[12] R. Vaidhyanathan, S. Natarajan C. N. R. Rao, Crystal Growth & Design, **2003**, 3, 47-51.

[13] C. Livage, C. Egger, G. Ferey, Chem. Mater. **2001**, 13, 410-414.

[14] R. Roque-Malherbe, F. Lugo, C. Rivera, R. Polanco and O.N.C. Uwakweh, Current Applied Physics **2015**, 15, 571-579

[15] V S. Pavan K. Neti, X. Wu, P. Peng, S. Deng and L. Echegoyen, RSC Adv., **2014**, 4, 9669–9672

[16] R. Roque-Malherbe, E. Carballo, R. Polanco, F. Lugo, and C. Lozano, J. Phys. & Chem.Solids, *2015*, 86, 65-73.

[17] R. Roque-Malherbe, R. Adsorption and Diffusion of Gases in Nanoporous Materials, CRC Press-Taylor & Francis, Boca Raton, FL, USA, **2007**.

[18] Roque-Malherbe, R., The Physical Chemistry of Materials: Energy and Environmental Applications, CRC Press, Boca Raton, Florida, **2010**.

[19] D. Cazorla-Amoros, J. Alcañiz-Monge, M.A. de la Casa-Lillo, C. Linares-Solano, Langmuir **1998**, 14, 4589-4596 (1998).

[20] R. Roque-Malherbe, O.N.C. Uwakweh, C.; Lozano, R. Polanco, A. Hernandez-Maldonado, P. Fierro, F. Lugo, J.N. Primera-Pedrozo, J. Phys. Chem. C **2011**, 115, 15555-15569.

[21] R. Roque-Malherbe, R. Polanco F. Marquez-Linares, J. Phys. Chem. C **2010** ,114, 17773-17787.

[22] R. Roque-Malherbe, C. Lozano, R. Polanco, F. Marquez, F. Lugo, A. Hernandez-Maldonado J.N. Primera-Pedroso, J. Solid State Chem. **2011**, 184, 1236-1244.

[23] V.A. Tvardoskiy. Sorbent deformation. The Netherland: Elsevier; 2006.

[24] V. Yu. Yakovlev, A.A. Fomkin, V.A. Tvardoskiy, , J. Coll. Int. Sci. V. Yu. **2006**, 268, 33-36.

25. F-X. Coudert, A. Boutin, M. Jeffroy, C. Mellot-Draznieks, A.H. Fuchs, ChemPhysChem **2011**, 12, 247-258.

26. A. Boutin, F-X. Coudert, M-A. Springuel-Huet, A. V. Neimark, G. Ferey, A.H. Fuchs, J. Phys. Chem. C **2011**, 114, 22237-22244.

[27] P.L. Llewellyn, G. Maurin, T. Devic, B. Loera-Serna, N. Rosenbach, V. Serre, S. Bourrelly, P. Horcajada, Y. Filinchuk, P. Ferey, J. Am. Chem. Soc. **2008**, 130, 12808-12814.

[28] K. Tan, N. Nijem, P. Canepa, Q. Gong, J. Li, T. Thonhauser, Y. Chabal, Chem. Mater. **2012**, 24, 3153−3167.

[29] A.M. Dwivedi, S. Krimm S. Mierson, , Spectrochim. Acta, **1989**, 45A, 271-279.

[30] B. Bonelli, B. Onida, B. Fubini, C. Otero-Arean, and E. Garrone, Langmuir **2000**, 16, 4976-4983.

[31] A.L. Goodman, L.M. Campus, K.T. Schroeder, Energy Fuels **2005**, 19, 471-476.

[32] F.X. Llabre´s i Xamena, A. Zecchina, Phys. Chem. Chem. Phys **2002**, 4, 1978–1982.

[33] P.L. Llewellyn, S. Bourrelly, C. Serre, A. Vimont, M. Daturi, L. Hamon, M. De Weireld, J-S. Chang, Hong, D-Y. Hwang, S.H. Jhung, G. Ferey, **2008**, 24, 7245-7250.

[34] C. Prestipino, L. Regli, J.G. Vitillo, F. Bonino, A. Damin, L. Lamberti, A. Zecchina, P.L. Solari, K.O. Kongshaug, S. Bordiga, Chem. Mater. **2006**, 18, 1337-1346.

[35] M. Zentkova, M. Mihalika, I. Toth, I. Z. Mitroovaa, A. Zentkoa, M. Sendeka, J. Kovac, M. Lukakpwa, M. Maryskoc, M. Miglierinib, J. Magnetism & Magnetic Mat. **2004**, 272–276, e753–e754

[36] B.N. Figgi, J. Lewis, J. in The Magnetic properties of transition metal complexes, in coordination chemistry, J, Lewis and R.S. Wilkins, eds. Wiley, **1960**, pp. 400-454.

[37] Hahn, T. (Ed.), International Tables for Crystallography (fifth edition), The International Union of Crystallography, Springer, Volume A **2009**,.

[38] W. Kraus W. G. Nolze, PowderCell-2.4, Federal Institute for Materials Research and Testing, Rudower Chaussee 5 Berlin, Germany, **2000**.

[39] M.M. Dubinin, Prog. Surf. Memb. Sci. **1975**, 9, 1-70.

[40] R. Roque-Malherbe, Mic. Mes. Mat., **2000**, 41, 227-240.

[41] B.P. Bering, V.V. Serpinskii, Bulletin of the Academy of Sciences of the USSR. Division of Chemical Sciences, **1974**, 23, 2342-2353.

[42] B.P. Bering, M.M. Dubinin, M.M. and V.V. Serpinskii, J. Coll. Int. Sci., 1972, 38, 185-194.

[43] H. Omi, T. Ueda, K. Miyakubo, T. Eguchi, App. Surf. Sci. **2005**, 252, 660-667.

[44] E.G. Derouane, in Zeolites Micropoorous Solids: Synthesis, Structure and Reactivity, E.G. Derouane, F. Lemos, C. Naccache, F. Ramos-Riveiro (eds.), Kluwer Academic Publishers, Dordrecht, **1992**. p. 511-524.

[45] Z. Amghouz, L. Roces, S. Garcıa-Granda, J.R. Garcıa, B. Souhail, L. Mafra, F. Shi, J. Rocha, J. Solid State Chem. **2009**, 182, 3365–3373.

[46] S. Ross, and J.P. Olivier, On Physical Adsorption, Wiley, New York, **1964**.

[47] A.D. Buckingham, R.L. Dish, Proc. Royal Soc. London A. **1963**, 273, 275-289.

**Table 1. Cell parameters of the degassed at 373 K, 448 K, 473 K and 523 K Cu-Su-MOF calculated with the Pawley method.**

| **Sample** | ***a* (Å)** | ***b* (Å)** | ***c* (Å)** | ***β*** | **$V_c$(Å$^3$)** |
|---|---|---|---|---|---|
| 373K | 8.171(1) | 8.647(1) | 9.284(1) | 86.02(2) | 654.1(1) |
| 448K | 8.139(1) | 8.645(1) | 9.437(1) | 87.66(2) | 663.2(1) |
| 473K | 8.143(1) | 8.637(1) | 9.416(1) | 87.51(2) | 661.3(1) |
| 523K | 8.130(3) | 8.651(2) | 9.521(2) | 88.14(4) | 669.8(5) |

**Table 2. Parameters calculated with the Langmuir type isotherm equation for low pressure $CO_2$ adsorption at 298 K on the Cu-Su-MOF degassed at 373 K, 448 K and 473 K**

| ***Temp.*** $[K]$ | $N_O^{CO_2}\ [mmol/g]$ | $W_O^{CO_2}\ [cm^3/g]$ |
|---|---|---|
| 373 | 1.99 | 0.096 |
| 448 | 2.17 | 0.105 |
| 473 | 2.73 | 0.131 |

**Table 3. Atomic positions, Wyckoff sites and occupancy factors for the dehydrated Cu-Su-MOF, with chemical formula $CuC_{12}O_{12}H_{18}$ (H was not included)**

| Site | x | Y | Z | Wyckoff site | Occupancy |
|---|---|---|---|---|---|
| Cu | 0 | 0 | 0 | 1 a | 1 |
| O1 | 0 | 0.17 | 0 | 2 c | 2 |
| O2 | 1 | 0 | 0.17 | 1 a | 1 |
| O3 | 1 | 0 | 0.83 | 1 a | 1 |
| O4 | 0.17 | 0 | 1 | 1 a | 1 |
| O5 | 0.83 | 0 | 1 | 1 a | 1 |
| O6 | 0.25 | 0 | 0.2 | 1 a | 1 |
| O7 | 0.75 | 0 | 0.2 | 1 a | 1 |
| O8 | 0 | 0.75 | 0.8 | 2 c | 2 |
| O9 | 0.8 | 0.75 | 0 | 2 c | 2 |
| C1 | 0.25 | 0 | 1 | 1 a | 1 |
| C2 | 0.75 | 0 | 1 | 1 a | 1 |
| C3 | 0.4 | 0 | 1 | 1 a | 1 |
| C4 | 0.6 | 0 | 1 | 1 a | 1 |
| C5 | 0 | 0.75 | 0.9 | 2 c | 2 |
| C6 | 0 | 0.6 | 0 | 2 c | 2 |
| C7 | 0.9 | 0.75 | 0 | 2 c | 2 |
| C8 | 1 | 0 | 0.6 | 1 a | 1 |
| C9 | 1 | 0 | 0.4 | 1 a | 1 |

**Table 4. Cell parameters of the degassed at 373 K, Cu-Su-MOF refined with the Rietveld method for the atomic positions and occupancy factors reported in Table 3.**

| **Sample** | ***a* (Å)** | ***b* (Å)** | ***c* (Å)** | ***β*** | **$V_c$(Å$^3$)** |
|---|---|---|---|---|---|
| 373K | 7.81 (8) | 8.58(4) | 9.89(3) | 83.0(7) | 657 (1) |

**Table 5. Parameters calculated with the Dubibin-Radushkevich (DR) equation for the high pressure $CO_2$ adsorption at 273 and 298 K on the Cu-Su-MOF degassed at 448 K.**

| ***Temp.*** $[K]$ | $N_{DR}^{CO_2}\ [mmol/g]$ | $E_{DR}^{CO_2}\ [kJ/mol]$ | $W_{DR}^{CO_2}\ [cm^3/g]$ | $q_{iso}^{DR}(0.37)\ [kJ/mol]$ |
|---|---|---|---|---|
| 273 | 4.44 | 24 | 0.217 | 28 |
| 298 | 4.85 | 25 | 0.255 | 29 |

**Figures:**

**Figure 1.** SEM images of the as-synthesized Cu-Su-MOF

**Figure 2**. XRD profiles of the as-synthesized (298 K) and degassed at 373 K, 448 K, 473 K and 523 K Cu-Su-MOF.

**Figure 3** DRIFTS spectra of the Cu-Su-MOF as-synthesized (298 K) and degassed at 373 K, 448 K and 523 K in the range between, 1800-3800 $cm^{-1}$ (a) and degassed at 448 and 523 K in the range between: 600-1800 $cm^{-1}$ (b)

**Figure 4.** DRIFTS spectrum of $CO_2$ adsorbed on degassed Cu-Su-MOF (b) (a) and Raman spectrum of the as-synthesized Cu-Su-MOF (b).

**Figure 5.** Magnetization curve of the as-synthesized Cu-Su-MOF and the Ni-nitroprusside used as standard.

**Figure 6**. Cu-Su-MOF, TG profile (a) and low pressure $CO_2$ adsorption at 298 K on the Cu-Su-MOF degassed at 373 K, 448 K and 473 K (b).

**Figure 7** Framework of the degassed Cu-Su-MOF along the [100], [001] and [010] crystallographic directions.

**Figure 8.** XRD profile of the dehydrated MOF simulated with the PowderCell software (a) and Rietveld fitting (b) of the XRD profile of the Cu-Su-MOF

**Figure. 9.** High pressure $CO_2$ adsorption-desorption isotherms (a), D-R plots of the high pressure adsorption data (b), Micropore volume ($W$) versus osmotic pressure ($\Pi$) at 273 K (c) and 298 K (d) and plot of the isosteric heat of adsorption versus $\theta$ (e).

**Fig. 1.**

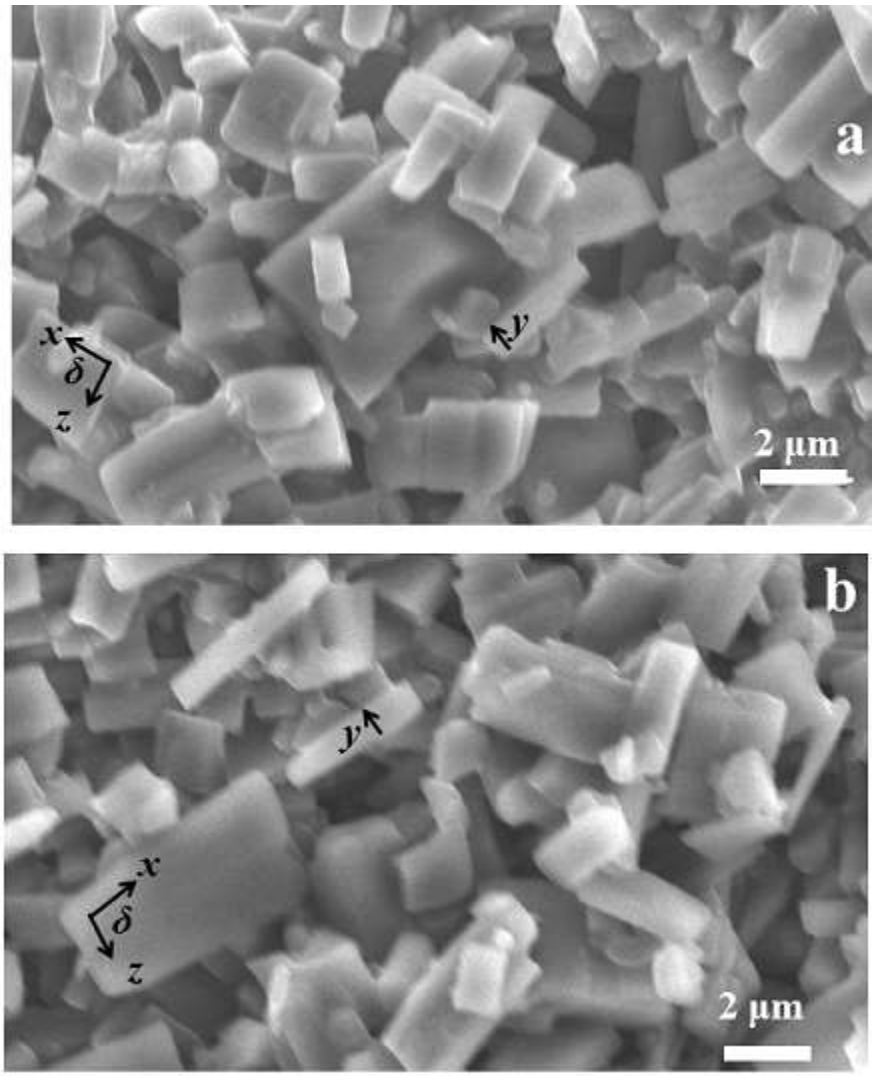

**Fig. 2.**

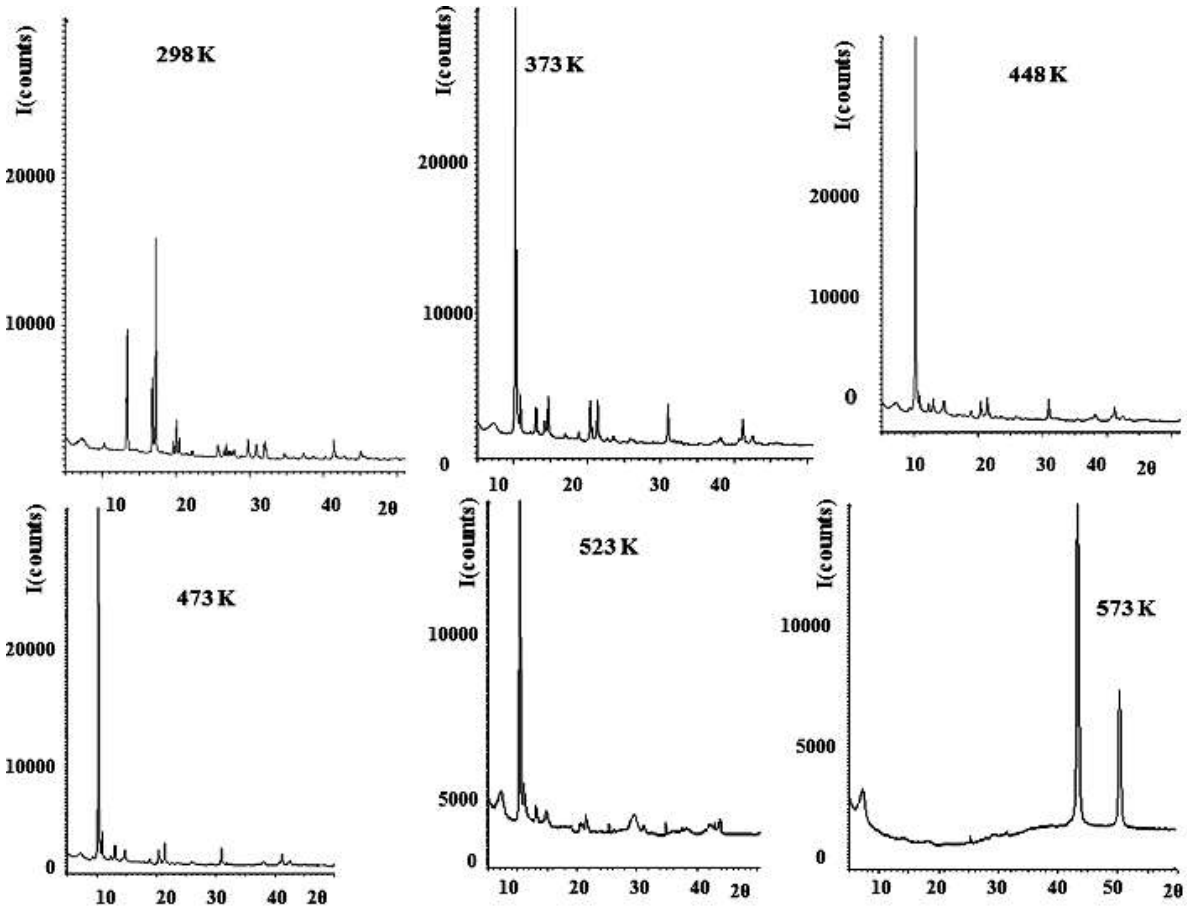

**Fig. 3.**

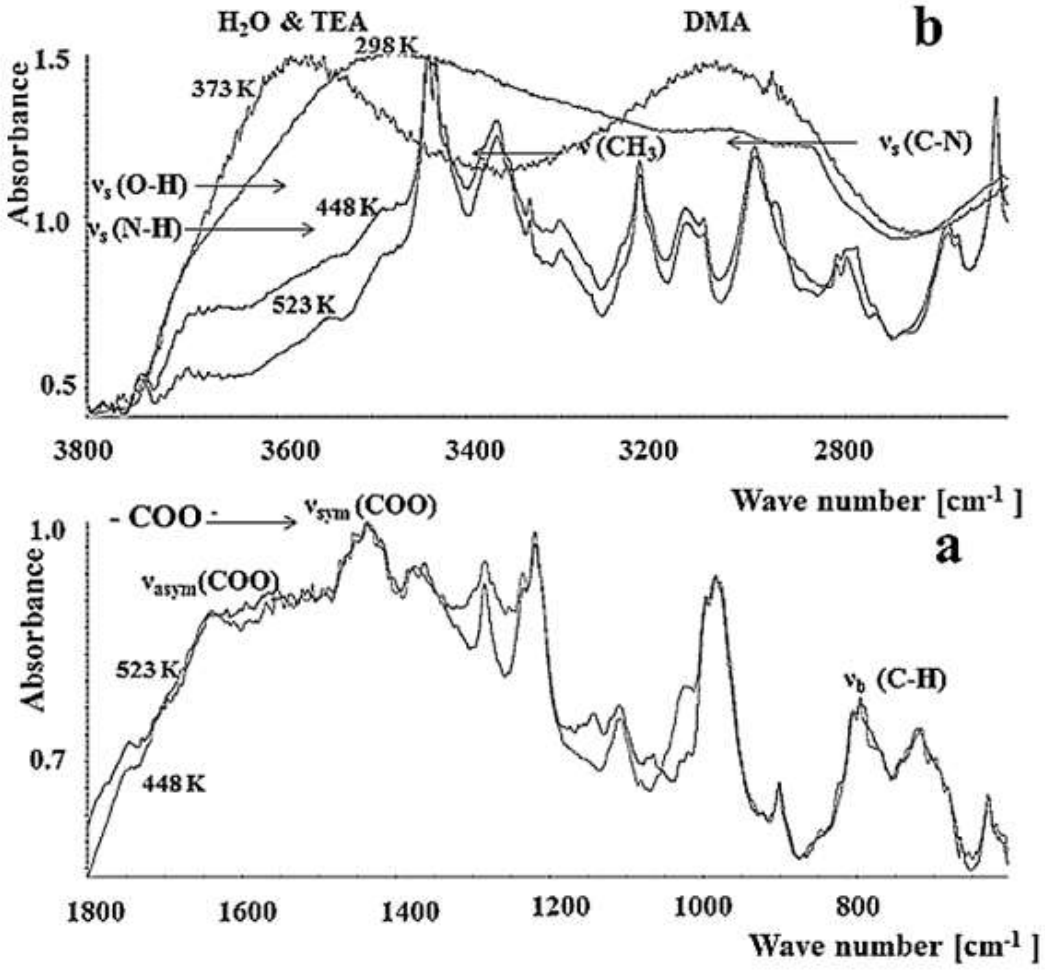
H2O & TEA
DMA
b
298 K
373 K
448 K
523 K
Absorbance
1.5
1.0
0.5
νs (O-H)
νs (N-H)
ν (CH3)
νs (C-N)
3800
3600
3400
3200
2800
Wave number [cm-1 ]
- COO -
νsym (COO)
νasym(COO)
a
1.0
0.7
523 K
448 K
νb (C-H)
1800
1600
1400
1200
1000
800
Wave number [cm-1 ]

**Fig. 4.**

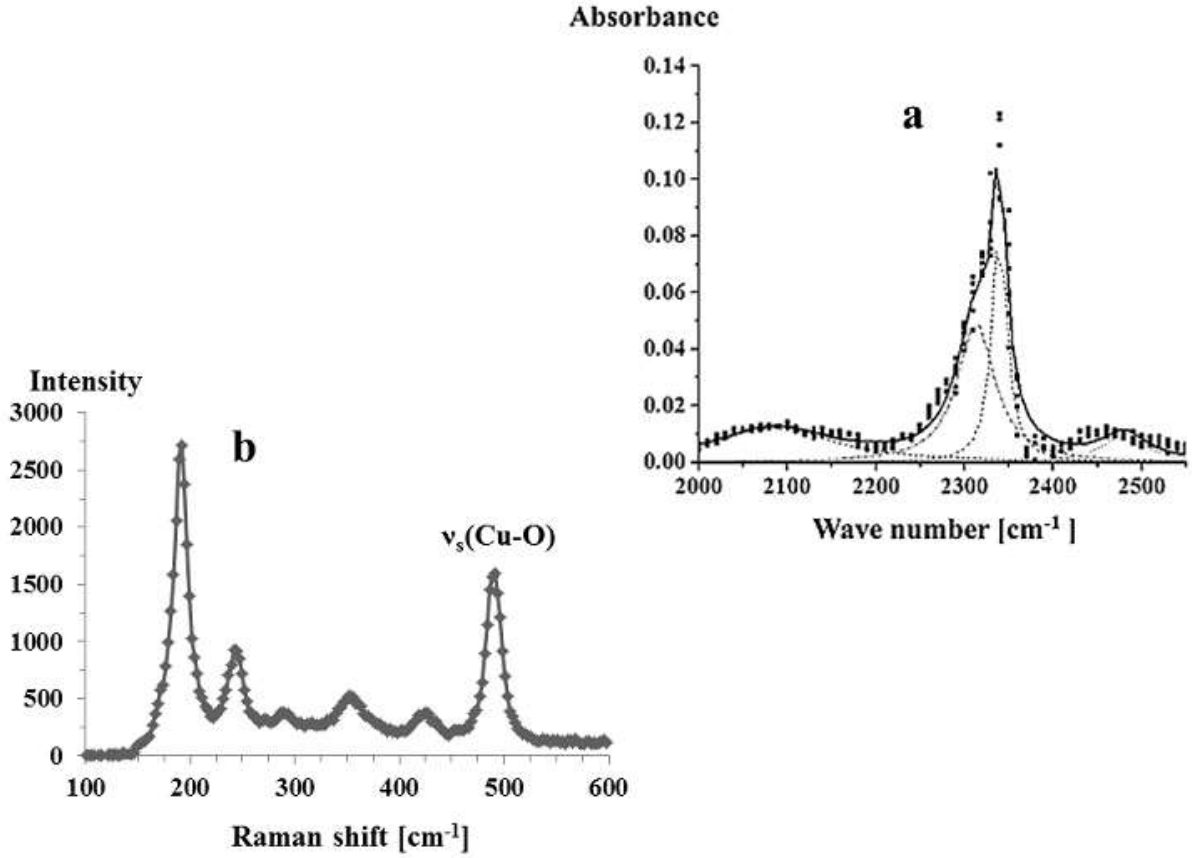
Absorbance
a
Wave number [cm-1 ]
Intensity
b
νs(Cu-O)
Raman shift [cm-1]

**Fig. 5**

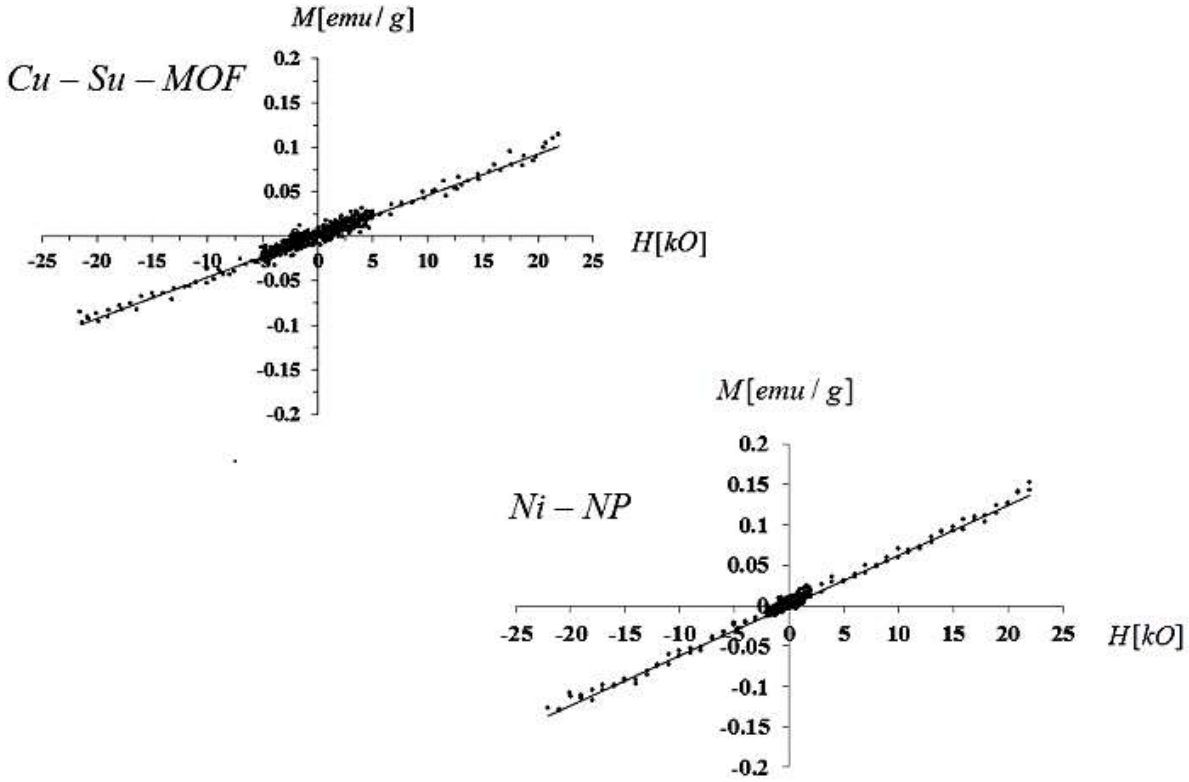
M[emu / g]
Cu – Su – MOF
0.2
0.15
0.1
0.05
-25 -20 -15 -10 -5 0 5 10 15 20 25
H[kO]
-0.05
-0.1
-0.15
-0.2
M[emu / g]
Ni – NP
0.2
0.15
0.1
0.05
0
-25 -20 -15 -10 -5 0 5 10 15 20 25
H[kO]
-0.05
-0.1
-0.15
-0.2

**Fig. 6.**

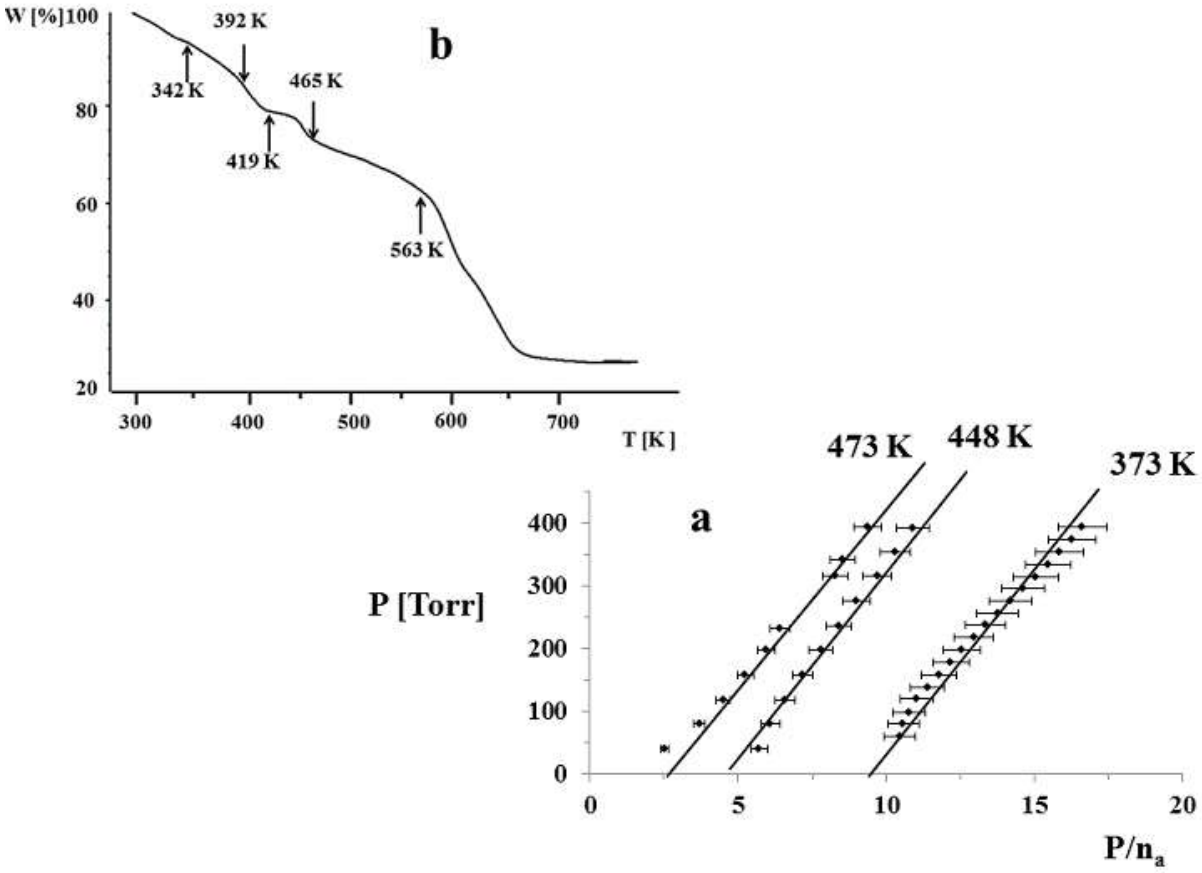
W [%]100
80
60
40
20
300
400
500
600
700
T [K]
b
392 K
342 K
465 K
419 K
563 K
473 K
448 K
373 K
a
P [Torr]
400
300
200
100
0
0
5
10
15
20
P/n_a

**Fig. 7**

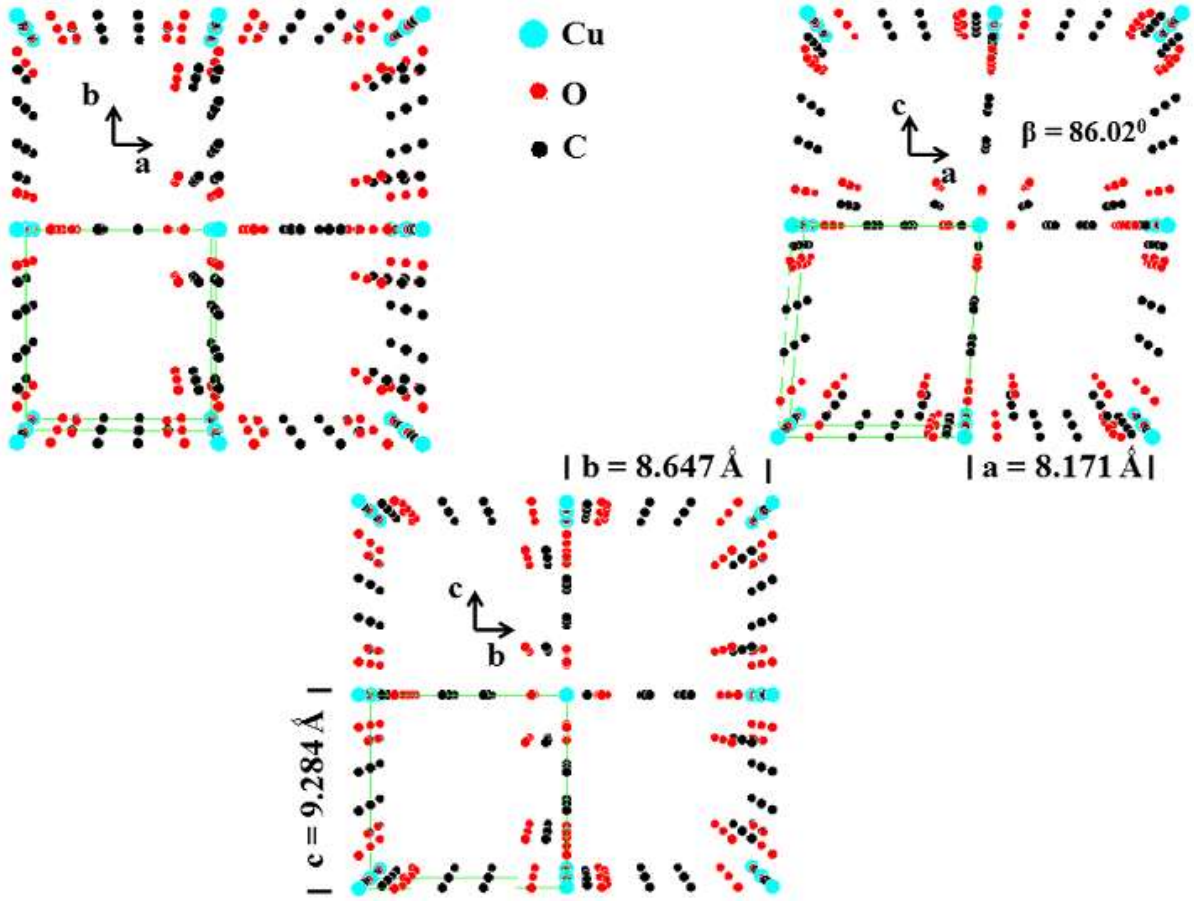

**Fig. 8.**

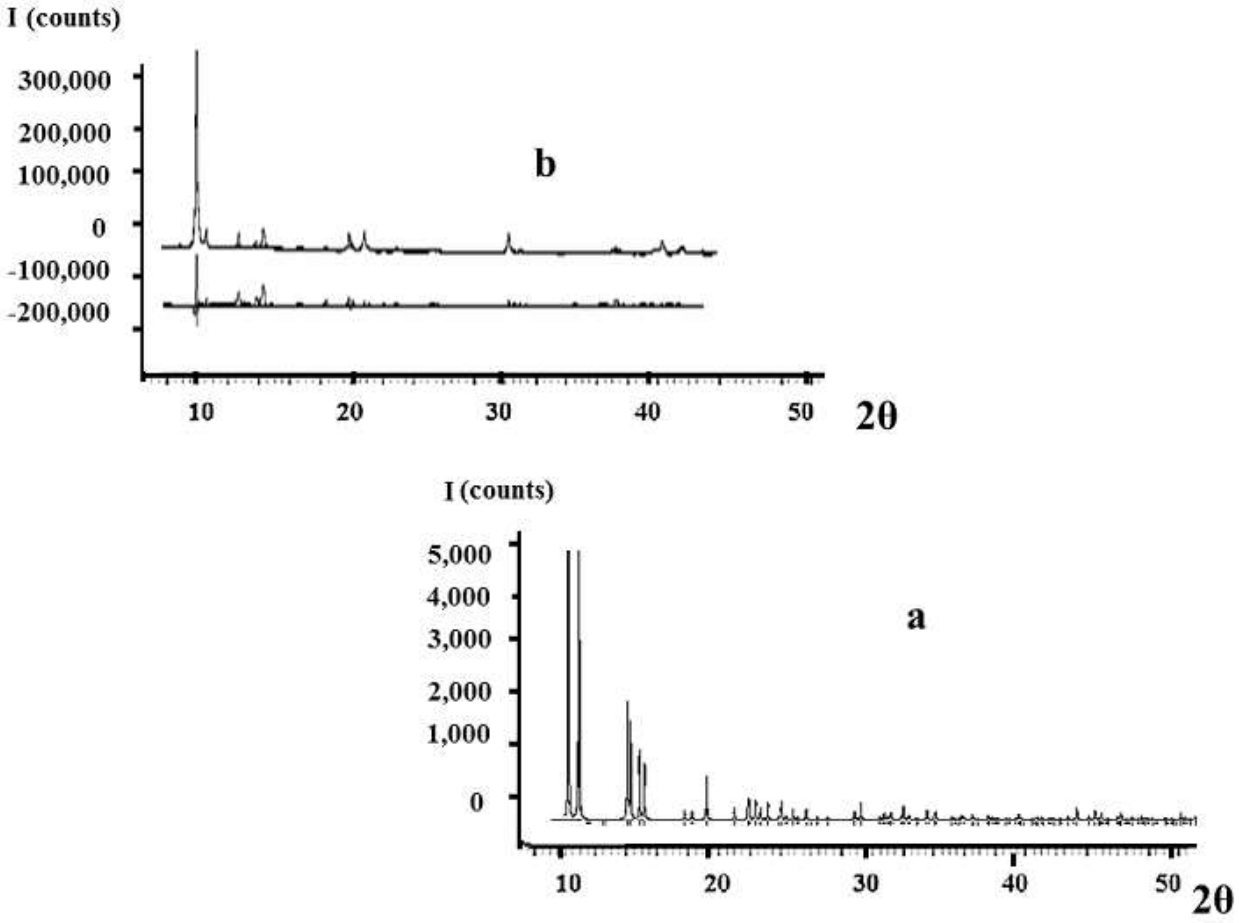
I (counts)
300,000
200,000
100,000
0
-100,000
-200,000
b
10
20
30
40
50
2θ
I (counts)
5,000
4,000
3,000
2,000
1,000
0
a
10
20
30
40
50
2θ

**Fig. 9.**

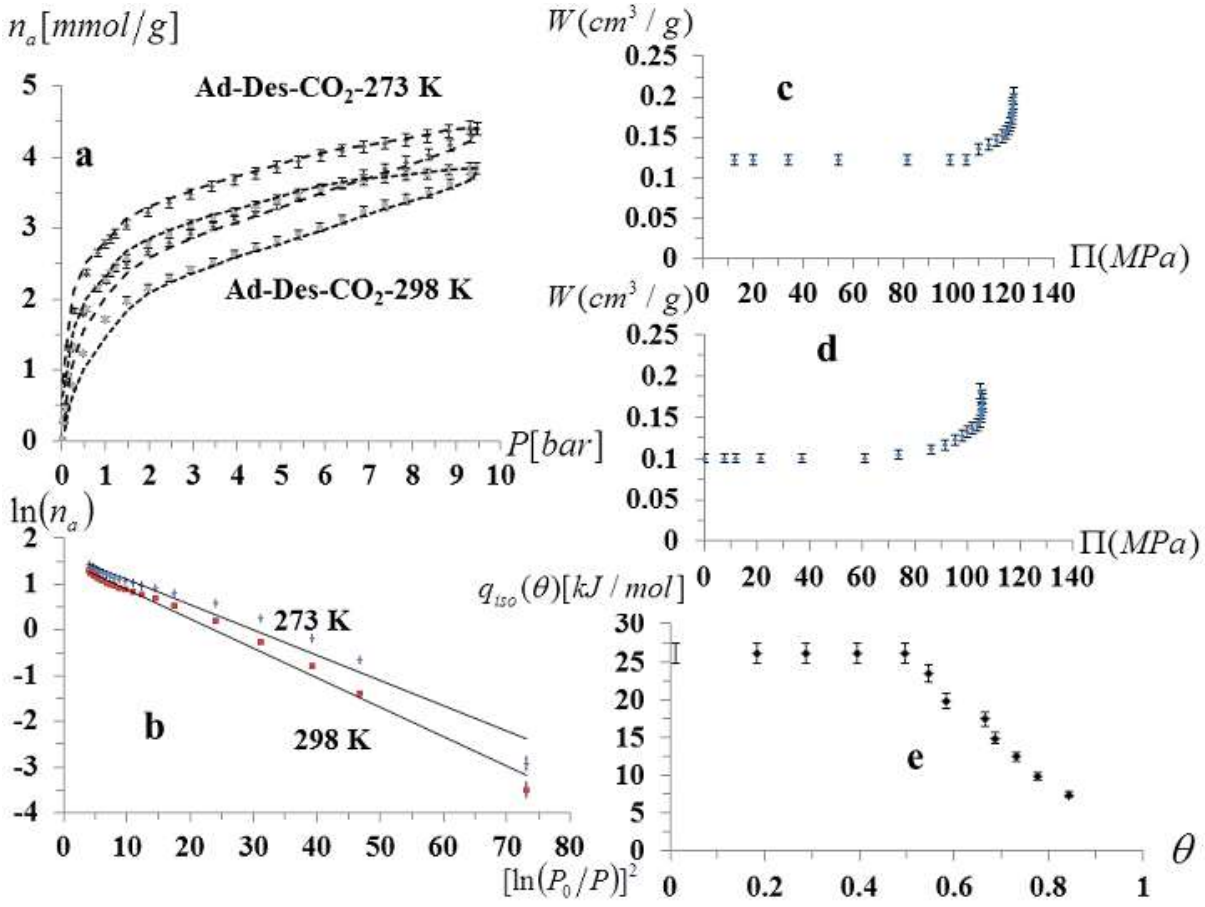
$n_a[mmol/g]$
Ad-Des-$CO_2$-273 K
a
Ad-Des-$CO_2$-298 K
$P[bar]$
$W(cm^3/g)$
c
$\Pi(MPa)$
d
$\ln(n_a)$
273 K
b
298 K
$[\ln(P_0/P)]^2$
$q_{iso}(\theta)[kJ/mol]$
e
$\theta$